THE JOURNAL OF BIOLOGICAL CHEMISTRY VOL. 286, NO. 22, pp. 20087–20099, June 3, 2011
Printed in the U.S.A.

Synergistic Interactions between Heregulin and Peroxisome Proliferator-activated Receptor-γ (PPARγ) Agonist in Breast Cancer Cells*[S]

Received for publication, October 5, 2010, and in revised form, April 1, 2011 Published, JBC Papers in Press, April 5, 2011, DOI 10.1074/jbc.M110.191718

Bae-Hang Park[‡§], Sean-Bong Lee[¶], Donna B. Stolz[‖], Yong J. Lee[‡], and Byeong-Chel Lee[‡§1]**

*From the [‡]University of Pittsburgh Cancer Institute, [§]Department of Medicine, Division of Hematology and Oncology, University of Pittsburgh School of Medicine, Pittsburgh, Pennsylvania 15213, [¶]Genetics of Development and Disease Branch, NIDDK, National Institutes of Health, Bethesda, Maryland 20892, and the Departments of [‖]Cell Biology and Physiology and **Surgery, University of Pittsburgh School of Medicine, Pittsburgh, Pennsylvania 15213*

Here, we demonstrate that troglitazone (Rezulin), a peroxisome proliferator-activated receptor agonist, acted in synergy with heregulin to induce massive cell death in breast cancer cells. Although the combination of heregulin and troglitazone (HRG/TGZ) induced both apoptosis and necrosis, the main mode of cell death was caspase-independent and occurred via necrosis. This combination increased generation of superoxide in mitochondria, which in turn destabilized mitochondria potential. Pretreatment with *N*-acetyl-L-cysteine and catalase expression ameliorated cell death induced by the combination treatment, indicating a role of oxidative stress in mediating HRG/TGZ-induced cell death. Notably, pretreatment with pyruvate significantly prevented the cell death, suggesting a potential mechanistic link between metabolic stress and HRG/TGZ-induced cell death. The activation of the HRG signaling axis has been considered as a poor prognostic factor in breast cancer and confers resistance to gefitinib (Iressa) and tamoxifen. However, our data presented here paradoxically suggest that HRG expression can actually be beneficial when it comes to treating breast cancer with peroxisome proliferator-activated receptor-γ ligands. Taken together, the combination of HRG and TGZ may provide a basis for the development of a novel strategy in the treatment of apoptosis-resistant and/or hormone-refractory breast cancer.

Breast cancer is the second most common cause of cancer death, accounting for one in three of all cancer cases diagnosed in women. Although overall survival continues to improve for breast cancer, intrinsic or acquired therapy resistance has been an ongoing obstacle to reducing overall breast cancer mortality. Combining different drugs is now widely used to overcome the problem of therapy resistance. Combination therapy often increases the likelihood of response, and in ideal combination may even be synergistic rather than simply additive. In addition, by keeping each drug at low dose, there can be the potential advantages of longer duration of action and less side effects.

Heregulin (HRG),[2] also known as neuregulin or neu differentiation factor, is a soluble secreted growth factor. The HRG gene family consists of four members, *HRG-1*, *HRG-2*, *HRG-3*, and *HRG-4*, of which a multitude of different isoforms are synthesized by alternative exon splicing (1). HRG binds to HER3 receptors or HER4 receptors, or both, resulting in the formation of receptor homo- and heterodimerization. In mammary epithelial cells, HRG predominantly uses HER2 and HER3 dimers. Upon engagement of HRG with the heregulin extracellular domain, multiple signaling pathways, such as the phosphatidylinositol 3-kinase (PI3K)/AKT, RAS/MAPK, and JNK pathways, are activated. To date, most studies have shown that HRG exhibits a growth-stimulatory effect in a variety of cancer cells, including breast cancer cells. Several lines of evidence implicated activation of human epidermal growth factor receptors by HRG as a primary driver of malignancy (2–4). Activation of HER-3 by HRG is also involved in resistance to current EGF receptor-targeted therapies (5). Furthermore, HRG induces the progression of breast cancer cells to more resistance to anti-estrogenic therapy and to a more aggressive phenotype (6).

Peroxisome proliferator-activated receptors (PPARs) belong to the nuclear hormone receptor superfamily and are implicated in the pathology of numerous diseases, including obesity, diabetes, atherosclerosis, and cancer (7). PPARs consist of α, β, and γ subtypes. Among PPARs, PPARγ is of particular interest, because it is expressed in many human cancers and plays key roles in the proliferation, differentiation, and apoptosis of cancer cells. Accordingly, PPAR activation in cancer has been intensively studied. Recent studies have shown that ligand activation of the PPARγ receptor causes growth inhibition by inducing the differentiation or apoptosis of various human cancer cells (8). Breast cancer cells often express prominent levels of PPARγ (9), and mice with germ line deletion of PPAR

* This work was supported, in whole or in part, by National Institutes of Health Grant CA140554 (to Y. J. L.). This work was also supported by Department of Defense Grant W81XWH-09-1-0350 and University of Pittsburgh Cancer Institute (to B.-C. L.).

[S] The on-line version of this article (available at http://www.jbc.org) contains supplemental Figs. 1–4.

[1] Recipient of a research scholar grant from The Hillman Foundation. To whom correspondence should be addressed: University of Pittsburgh Cancer Institute, Hillman Cancer Center, 5117 Centre Ave., Pittsburgh, PA 15213. Tel.: 412-623-2285; Fax: 412-623-7828; E-mail: leeb4@upmc.edu.

[2] The abbreviations used are: HRG, heregulin; TGZ, troglitazone; Z, benzyloxycarbonyl; fmk, fluoromethyl ketone; PPAR, peroxisome proliferators activated receptor; NAC, *N*-acetylcysteine; ROS, reactive oxygen species; PPRE, PPAR response element; 3-MA, 3-methyladenine; MePyr, methyl pyruvate; NaPyr, sodium pyruvate; PI, propidium iodide; PARP, poly(ADP-ribose) polymerase.

(PPAR$^{+/-}$) have a greater susceptibility to breast cancer (10), suggesting a strong causal link between PPARγ and progression of breast cancer.

Among PPARγ ligands, troglitazone (Rezulin, Resulin, or Romozin) (TGZ), the most extensively studied compound, shows anti-tumorigenic effects in human breast cancer cells (9, 11). TGZ also exerts its anti-tumorigenic effects in colon cancer cells both *in vivo* and *in vitro* (12). However, there have been some apparently contradictory observations in which TGZ treatment increases the number of precancerous polyps in the colon in Apc mutant mice compared with untreated ones (13, 14). It was also reported that activation of PPARγ signaling enhances mammary tumorigenesis via activation of Wnt signaling (15). Furthermore, TGZ has been shown to stimulate growth of osteosarcoma (16), suggesting that TGZ can trigger both stimulatory and inhibitory effects depending on the cell- and tissue-specific context (7).

Although there have been trials with the use of PPARγ agonists in the treatment of cancer, such treatment was not successful as a monotherapy in breast (17) and colorectal cancer (18). In a recent study by Girnun *et al.* (19), combining a platinum-based drug, carboplatin, with *PPARγ* ligands is showing highly promising results in inhibition of lung, colon, and ovarian cancer cell growth. However, platinum-based drugs, including carboplatin, are not normally used to treat breast cancer (20), although there is an ongoing trial using platinum-based therapy in triple-negative breast cancer patients who do not harbor a *BRCA1* mutation (21).

TGZ, although it is one of the most extensively studied PPARγ agonists, has recently been withdrawn from clinical trials because of its hepatocyte toxicity. Rosiglitazone (Avandia), another PPARγ agonist, is still on the market, but the cardiovascular safety of rosiglitazone is currently the subject of vigorous debate, necessitating further efforts to minimize its side effects. Hence, there is a compelling need to seek alternative combinatorial therapies to target breast cancer with PPARγ ligands.

Both HRG and TGZ have been found to exert not only *inhibitory* but also *stimulatory* effects on breast cancer cell growth. In this study, we demonstrate that these two-faced molecules, when combined, exert a pronounced synergy on cell death in breast cancer cells. We also explore molecular mechanisms by which these two compounds synergistically induce cell death in breast cancer cells.

EXPERIMENTAL PROCEDURES

Reagents—Recombinant human heregulin β-1 was purchased from PeproTech (Rocky Hill, NJ). Troglitazone, *N*-acetylcysteine, 3-methyladenine, propidium iodide (PI), E64d, and pepstatin A were obtained from Sigma. p38 MAPK inhibitor SB 203580, JNK inhibitor SP 600125, PI3K inhibitor LY 294002, PPARγ antagonist, GW9662, IM-54, and Z-VAD-fmk were purchased from Calbiochem. FuGENE HD and cell death detection ELISA kit were purchased from Roche Applied Science. Z-VAD-fmk and Dual-Luciferase assay system were purchased from Promega (Madison, WI). MitoSOX and YO-PRO1 kits were obtained from Invitrogen.

Antibodies—Monoclonal anti-PARP antibody was purchased from Biomol International LP (Plymouth Meeting, PA). Polyclonal and monoclonal anti-H2AX were purchased from Millipore (Billerica, MA). Antibodies against either phosphorylated or unphosphorylated p38 MAPK, JNK, AKT, and ERK were purchased from Cell Signaling Technologies (Billerica, MA). Polyclonal anti-actin antibody was obtained from StressGen Bioreagents (Victoria, Canada). Polyclonal anti-catalase antibody was purchased from Calbiochem. Polyclonal anti-LC3 antibody was purchased from Novus Biologicals (Littleton, CO). Polyclonal anti-ATG7 antibody was obtained from Sigma.

Cell Culture—The human breast cancer cell lines MCF-7, SKBR-3, and MDA-MB-453 were grown in complete medium, containing DMEM, McCoy5A, and RPMI 1640, respectively, supplemented with 10% fetal bovine serum (Sigma). MCF-10A cell line was grown in DMEM/F-12 (Invitrogen) supplemented with 5% horse serum 20 ng/ml EGF (PeproTech, Rocky Hill, NJ), 100 ng/ml cholera toxin (Sigma), and 0.5 μg/ml hydrocortisone (Sigma). Unless otherwise stated, cells were grown to ~60% confluence, serum-starved overnight, and then treated with heregulin β-1 (100 ng/ml) and/or troglitazone (10 μM). When *N*-acetylcysteine, kinase inhibitors, or PPARγ antagonist were used, cells were pretreated with these reagents for 1 h before the addition of heregulin and/or troglitazone. MCF-7 cell line was infected with adenoviral vectors containing by human catalase for 4 h before heregulin and/or troglitazone treatment. The human catalase-expressing adenovirus was further purified and concentrated by Vivapure AdenoPACK (purchased from Sartorius, Goettingen, Germany).

Luciferase Reporter Assay—MCF-7 cells were transiently transfected with PPRE-luciferase reporter construct as well as pRL-SV40 *Renilla* internal control plasmid. After 16 h of transfection, cells were treated as indicated in the figure legends for another 24 h. Luciferase assay was performed 48 h after the transfection. Luciferase activity was normalized with control *Renilla* luciferase expression. Normalized luciferase activities of treated cells were expressed as fold increase compared with the untreated cells transfected with the same plasmid, arbitrarily set at 1. Experiments were done in duplicate, and the standard deviation was indicated.

Apoptosis/Necrosis Assay—Apoptosis was measured by the quantification of the histone-complexed DNA fragments (mono- and oligonucleosomes) by ELISA (Roche Applied Science). Lysates from cells treated similarly to those described above were analyzed. The level of mono- and oligonucleosomes released into the cytoplasm was measured at 405 nm against reference wavelength (460 nm). Enrichment factor was calculated as the ratio of the sample cells to the absorbance of control cells as described previously (22, 23) using the following formula: enrichment factor = milliunits (absorbance (10^{-3})) of the samples (apoptotic cells)/milliunits of the corresponding control. To assess apoptosis and necrosis, cells were stained with YO-PRO-1 and PI as directed by the manufacturer (Molecular Probes, Eugene, OR) and analyzed by flow cytometry (24, 25).

Mitochondrial Assays—Mitochondrial ROS levels were quantified as described by the manufacturer. MCF-7 cells were seeded into 6-well plates and cultured overnight followed by

serum starvation. The cells were then incubated with heregulin-β1 and/or troglitazone for the indicated periods of time. Before harvesting, cells were incubated with MitoSOX (final concentration, 5 μM) for 10 min. Cells were washed with PBS, collected, and kept on ice in the dark for immediate detection with a flow cytometer (Coulter Epics XL flow cytometer). For measurement of mitochondrial membrane potential, the mitochondrial membrane potential detection kit was used as instructed by the manufacturer (Cayman Chemical, Ann Arbor, MI). Cells were treated as above and incubated with 10 μg/ml JC-1 for 10 min, and then fluorescence was measured on a flow cytometer using FL1 and FL2 channels.

Electron Microscopy—Electron microscopy was performed as described previously (26). Briefly, MCF-7 cells grown in tissue culture dishes and treated as above were fixed with 2.0% paraformaldehyde, 2.5% EM grade glutaraldehyde in PBS. After fixation, samples were dehydrated in a graded series of ethyl alcohol and embedded. Ultrathin sections of samples were placed on copper grids and stained with uranyl acetate and lead citrate. Sections were examined under a JEM 1011CX electron microscope (JEOL, Peabody, MA).

Immunocytochemistry—MCF-7 cells were seeded onto coverslips in 6-well plates to obtain ~60% confluence and then treated as described above. The cells were then incubated with anti-phospho-H2AX (Ser-139) mouse monoclonal antibody at room temperature for 1 h followed by Alexa Fluor 488-conjugated anti-mouse IgG antibody (Molecular Probes Inc., Eugene, OR). Cells were then stained with DAPI (Molecular Probes Inc.). Cells were co-stained with antibodies to LC3, cytokeratin, and DAPI. Autophagy was quantified by counting the cells showing accumulation of *LC3* puncta as described previously (27). Images were captured using a Zeiss Axioskop fluorescent microscope with Plan-NeoFluar 63×/1.25 oil lens and a CoolSnapPro (Media Cybernetics) digital camera with associated software.

Measurement of Intracellular ATP—ATP levels were measured using a luminescence ATP detection system (PerkinElmer Life Sciences) according to the manufacturer's instructions. Luminescence was measured using Wallac microplate luminescence reader (PerkinElmer Life Sciences) as counts/s and normalized to total protein concentration for each sample. The relative ATP level was calculated by dividing the counts/s of the treated samples by that of the control samples.

RNA Interference—MCF-7 cells were transfected with 100 nM pooled small interference RNA (siRNA) oligonucleotide (SMART pool) against ATG7 (obtained from Dharmacon, Lafayette, CO) or with 100 nM nontargeting siRNA (siGENOME 5, Dharmacon, Lafayette, CO) by Dharmafect I (Dharmacon, Lafayette, CO) according to the manufacturer's instructions. The knockdown effect was examined by Western blot.

RESULTS

Combinatory Treatment of HRG and TGZ Markedly Increases Cell Death in Breast Cancer Cells—Both HRG and TGZ are well known differentiation-inducing factors in breast cancer cells. In agreement, HRG or TGZ alone induced differentiation of MCF-7 breast cancer cells, as determined by Oil Red O staining. However, combinatorial treatment with HRG and TGZ (HRG/TGZ) did not increase the extent of differentiation, compared with either HRG or TGZ alone (data not shown). Rather, *HRG/TGZ* treatment led to a significant cell death, as shown in Fig. 1*a*. To measure the extent of cell death, MCF-7 cells were stained by PI and assessed by flow cytometry. HRG alone and TGZ alone induced cell death at 48 h of treatment, but their effects were modest. However, when HRG and TGZ were combined, this markedly increased cell death at 48 h of treatment (Fig. 1*b*) and led to virtually complete cell death at 72 h of treatment (data not shown). PARP has been widely used as an early indicator of apoptotic cell death, and its cleaved protein (89 kDa) is correlated with the extent of apoptotic cell death. As shown in Fig. 1*c*, compared with samples from control, TGZ alone, or HRG alone, HRG/TGZ treatment resulted in an increase in the ratio of cleaved to uncleaved PARP. To test whether the effect of HRG/TGZ on MCF-7 cells was not a cell line-specific effect, we assessed how other breast cancer cell lines respond to HRG/TGZ treatment. Apoptotic cell death was measured by the quantitative detection of mono- and oligonucleosomes (histone-associated DNA fragments) in the cytoplasmic fraction of cell lysates by ELISA. Combinatory treatment of TGZ and HRG significantly increased apoptotic cell death in both SKBR-3 and MDA-MB-453 breast cancer cells as compared with either alone (Fig. 1*d*), suggesting that HRG/TGZ-induced apoptosis is not a cell line-specific phenomenon. Notably, although MCF-10A cell (normal-like diploid human breast epithelial cell line) was highly sensitive to TGZ alone as reported previously (28), it displayed a significant resistance to HRG/TGZ-induced apoptosis (Fig. 1*e*).

Signaling Pathways Involved in HRG/TGZ-induced Cell Death—HRG activates a vast number of signal transduction pathways. Among these pathways, we focused AKT, ERK, p38 MAPK, and JNK, which are known to regulate proliferation and apoptosis of breast cancer cells. HRG alone and HRG/TGZ induced a transient increase in phosphorylation of p38 MAPK, JNK, AKT and ERK in MCF-7 cells, with a peak activation occurring at 5 min (Fig. 2*a*). Compared with HRG alone, HRG/TGZ treatment sustained these activations over longer periods of time. Of note, HRG/TGZ treatment significantly augmented the late phase p38 MAPK activation compared with either TGZ or HRG alone (Fig. 2*a*). It has been previously documented that the late phase of p38 MAPK activation followed by HRG treatment is correlated with HRG-induced apoptotic cell death in breast cancer (29).

This suggests that the observed cell death in HRG/TGZ-treated cells might be attributed to the augmented late phase p38 MAPK activation. The kinetics of AKT, ERK, JNK, and p38 MAPK activation in MDA-MB-453 and SKBR-3 cells were also comparable with that of MCF-7 cells, although the late phase p38 MAPK activation was observed at earlier time points in these cells compared with MCF-7 cells (data not shown). To further elucidate which signaling pathways mediate HRG/TGZ-induced apoptotic cell death, we examined the effect of various chemical inhibitors on HRG/TGZ-induced apoptosis. Pretreatment with PI3K/AKT inhibitor (LY 294002), JNK inhibitor (SP 600125), or MEK/ERK inhibitor (U1026) did not exert any protective effects against HRG/TGZ-induced apo-

ptosis (data not shown). In contrast, p38 MAPK inhibitor SB 203580 decreased HRG/TGZ-induced apoptosis by about 35–40% (Fig. 2*b*), suggesting that p38 MAPK signaling is linked in part to HRG/TGZ-induced apoptosis.

We next determined the effects of the early and late phase of p38 MAPK activation on HRG/TGZ-induced apoptosis. Blocking the early phase of p38 MAPK activity (SB 203580 was retrieved before the onset of the late phase activation) provided

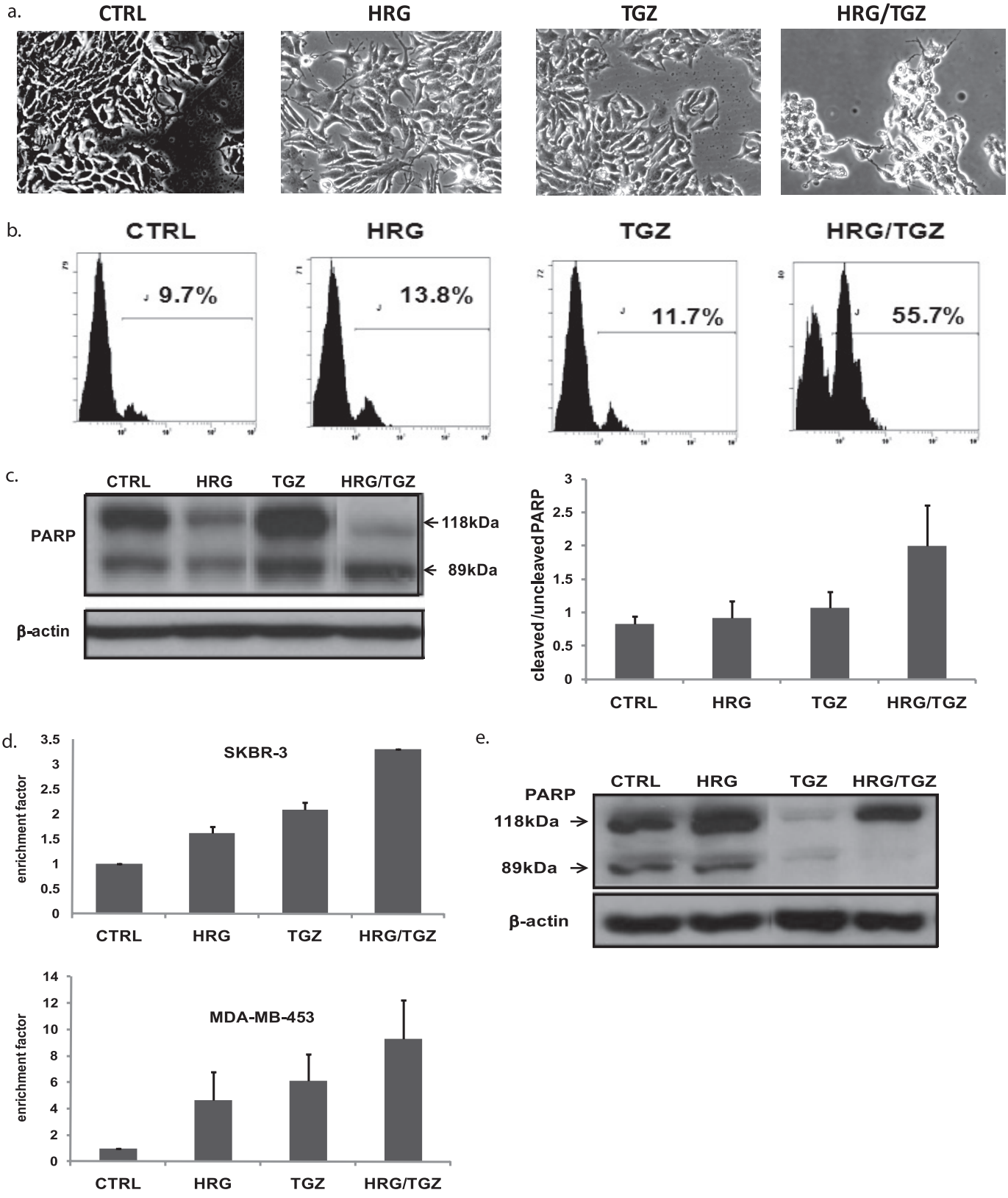

only modest protection from HRG/TGZ-induced apoptosis, as determined by PARP cleavage (Fig. 2*c*). SB 203580 is a reversible inhibitor (30). Therefore, even after the early phase p38 MAPK activation was inhibited by SB 203580, the late phase p38 MAPK activity was still fully reversible upon removal of the inhibitor as shown in Fig. 2*c* (*right lane, middle panel*). Contrary to the early phase blockade, blocking of the late phase p38 MAPK activation significantly reduced the extent of HRG/TGZ-induced PARP cleavage (Fig. 2*c*, *top panel, middle lane*), suggesting that the late phase of p38 MAPK activity plays a more significant role than the early phase activation in HRG/TGZ-induced apoptosis.

PPARγ activation plays a major role in apoptosis in cancer cells. To investigate whether HRG/TGZ induces synergistic activation of the PPARγ receptor and thus triggers apoptosis, we assessed PPARγ activity using PPRE luciferase reporter construct. The combination of TGZ and HRG could stimulate the promoter activity to a higher level compared with TGZ or HRG alone (Fig. 2*d*). However, increased PPARγ activity did not correlate with HRG/TGZ-induced apoptosis, because pretreatment of GW9662, a potent antagonist of PPARγ, did not alter the extent of apoptotic cell death induced by HRG/TGZ (data not shown). Although HRG/TGZ treatment enhanced PPARγ activity also in MDA-MB-453 and SKBR-3 cells, GW9662 was not able to rescue these cells either (data not shown). As such, these data suggest that HRG/TGZ exerts its action through PPARγ-independent pathways.

HRG/TGZ Induces Both Apoptotic and Nonapoptotic/Necrotic Cell Death—Given the central role of caspases in mediating apoptosis, we tested whether a pan-caspase inhibitor, Z-VAD-fmk, could prevent or attenuate HRG/TGZ-induced cell death. Z-VAD-fmk efficiently blocked HRG/TGZ-induced apoptosis (Fig. 3*a*), as determined by nuclear fragmentation. However, a major portion of HRG/TGZ-treated cells still underwent cell death, suggesting that nonapoptotic/necrotic mechanisms contribute to the HRG/TGZ-induced cell death.

To assess the extent of apoptosis and necrosis caused by HRG/TGZ treatment, HRG/TGZ-treated cells were stained with PI and YO-PRO-1. Viable cells with intact membrane exclude both dyes (live cells, YO-PRO-1−, and PI−), whereas apoptotic cells are permeable to YO-PRO-1, yet remain impermeable to PI (YO-PRO-1+, PI−) (31). Meanwhile, necrotic (or late apoptotic) cells lose membrane integrity and become PI-positive. HRG/TGZ induced both apoptotic and necrotic cell death, but mostly through the necrotic (62%) rather than the apoptotic (13%) pathway (Fig. 3*b*, *left panel*). Necrotic cell death can be better defined by electron microscopy. The majority of the HRG/TGZ-treated cells displayed typical changes associated with necrotic cell death, such as discontinuities in plasma membrane, multiple large vacuoles, and leakage of cellular contents (Fig. 3*c, left panel*). The percentages of apoptosis- and necrosis-like cells based on electron microscopic determination were comparable (Fig. 3*c*, *right panel*) with those obtained using YO-PRO-1/PI staining. Furthermore, IM-54, a selective inhibitor of oxidative stress-induced necrotic cell death, substantially reduced HRG/TGZ-induced cell death (supplemental Fig. 1), supporting the notion that HRG/TGZ-induced cell death occurred primarily through necrosis.

Notably, pretreatment of methyl pyruvate significantly reduced the extent of HRG/TGZ-induced necrosis (from 62 to 31%) with minimal impact on HRG/TGZ-induced apoptosis (Fig. 3*b*, *middle panel*), suggesting that HRG/TGZ-induced cell death is associated with metabolic stress. A comparable protective effect was also achieved with sodium pyruvate (HRG/TGZ + NaPyr) (data not shown). Of note, HRG/TGZ treatment resulted in marked depletion of cellular ATP levels compared with untreated cells (Fig. 3*d*). In contrast, supplementation of MePyr or NaPyr prevented HRG/TGZ-induced depletion of cellular ATP (Fig. 3*d*). These results suggest that pyruvate rescues the low energy status of HRG/TGZ-treated cells, further supporting the hypothesis that HRG/TGZ-induced cell death is mainly caused by metabolic stress. Low ATP concentration pushes the cell into necrotic cell death (11, 15), which is consistent with the major type of cell death observed in HRG/TGZ-treated cells.

The medium in the HRG/TGZ-treated wells precipitously turned yellow with a concomitant drop in pH (Fig. 3*e*) before the onset of cell death, reinforcing the causal association between HRG/TGZ-induced cell death and metabolic stress. Meanwhile, 3-MA, an autophagy inhibitor (HRG/TGZ + 3-MA), showed only modest effects on HRG/TGZ-induced necrosis (from 62 to 69%) (Fig. 3*b*, *right panel*).

Combinatory Treatment of HRG and TGZ Causes Oxidative Stress and Mitochondrial Dysfunction—Mitochondria play a major role in cellular energy metabolism, and metabolic stress can induce mitochondrial dysfunction (32). To test whether HRG/TGZ-induced cell death was associated with mitochondrial function, a change in mitochondrial transmembrane potential ($\Delta\psi_m$) was assessed by flow cytometric assessment of JC-1. JC-1 offers more reliable staining than rhodamines and other carbocyanines, because it can selectively enter into mitochondria (33). HRG alone had a slightly protective effect on

FIGURE 1. **Combination treatment of HRG and TGZ markedly increases cell death in breast cancer cells.** *a,* MCF-7 cells were treated for 48 h with either 100 ng/ml HRG or 10 μM TGZ alone or with a combination of heregulin and troglitazone (*HRG/TGZ*). Cell morphology was examined under the phase contrast microscope. *b,* quantification of cell death was made by PI staining (5 μg/ml). MCF-7 cells were treated for 48 h with either HRG or TGZ alone or with a combination of HRG/TGZ as described. The percentage of PI-positive cells indicates the proportion of cell death. Shown are representatives of at least three independent experiments. *c, left panel,* after treatment with the indicated compounds for 48 h, cell extracts from MCF-7 cells were prepared and analyzed by Western blotting using anti-PARP antibody. Shown is a representative Western blot of four independent experiments. *Right panel,* quantitative data expressing the ratio of cleaved to uncleaved PARP. PARP cleavage was quantified by densitometry, normalized to β-actin, and calculated as a ratio of cleaved PARP to uncleaved PARP. The data are expressed as the means ± S.E. *CTRL*, control. *d,* cells (SKBR-3 and MDA-MB-453) were treated as described in the legend to *a*. Cell death detection ELISA was used to measure apoptotic cell death. Rate of apoptosis is reflected by the enrichment of nucleosomes released in each sample. The ratio of the absorbance of the treated cells to the untreated cells (*CTRL*) was calculated as an enrichment factor. Data represent the means ± S.E. *e,* MCF-10A cells were treated as described in the legend to *a*. After treatment with the indicated compounds for 48 h, cell extracts were prepared and analyzed for PARP cleavage. Of note, PARP cleavage was not detectable in TGZ-treated MCF-10A cells, most likely because most of the TGZ-treated MCF-10A cells already died by the 48 h of TGZ treatment.

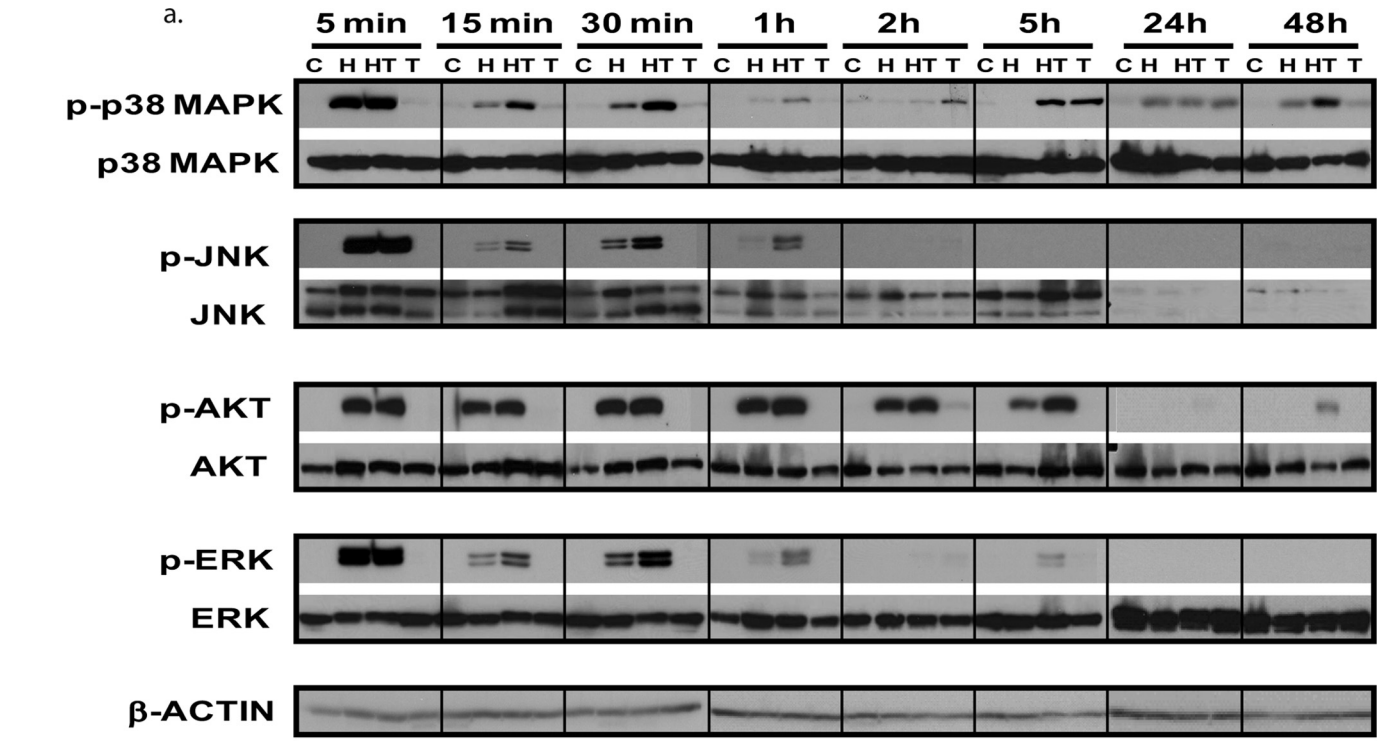
a.
5 min
15 min
30 min
1h
2h
5h
24h
48h
C H HT T
p-p38 MAPK
p38 MAPK
p-JNK
JNK
p-AKT
AKT
p-ERK
ERK
β-ACTIN

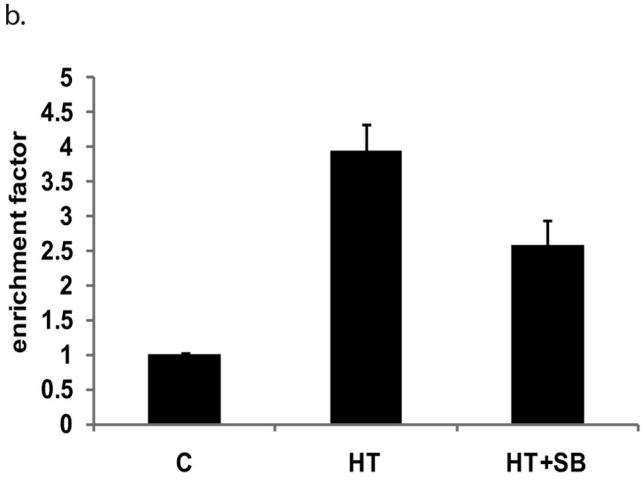
b.
enrichment factor
5
4.5
4
3.5
3
2.5
2
1.5
1
0.5
0
C
HT
HT+SB

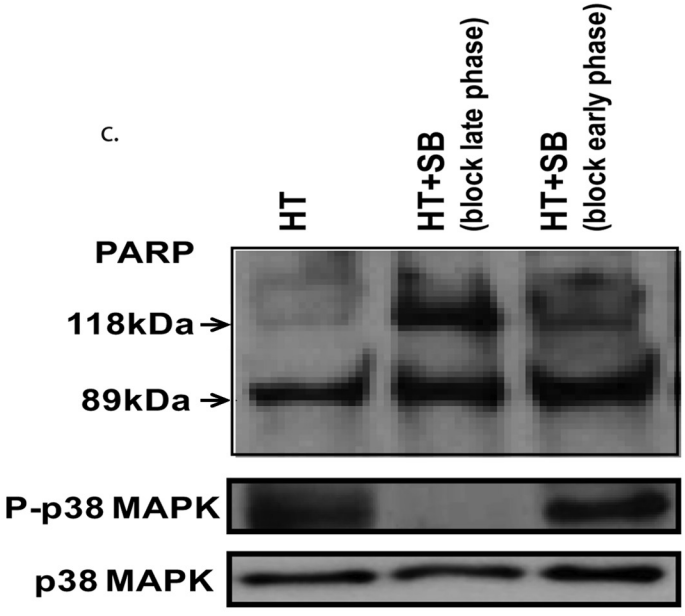
c.
HT
HT+SB (block late phase)
HT+SB (block early phase)
PARP
118kDa
89kDa
P-p38 MAPK
p38 MAPK

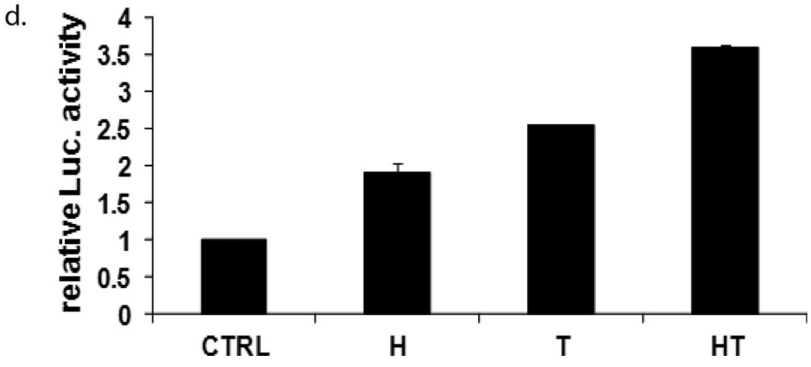
d.
relative Luc. activity
4
3.5
3
2.5
2
1.5
1
0.5
0
CTRL
H
T
HT

$\Delta\psi_m$, whereas TGZ alone destabilized $\Delta\psi_m$ (Fig. 4*a*). The combined treatment (HRG/TGZ) resulted in a further reduction in the mitochondrial transmembrane potential as indicated by a marked shift in JC-1 fluorescence (Fig. 4*a*).

ROS are postulated to be a common trigger for mitochondrial dysfunction. Therefore, we asked whether HRG/TGZ treatment causes an accumulation of higher levels of ROS, which in turn leads to the ROS-induced collapse of mitochondrial membrane potential. Because mitochondria are the primary source of ROS in eukaryotic cells, we measured mitochondrial ROS using MitoSox, which is a highly selective probe for mitochondrial superoxide anion. A higher level of mitochondrial ROS was observed in HRG/TGZ-treated cells than those treated with either alone or nontreated cells (Fig. 4*b*). Taken together, these results suggest that oxidative damage of mitochondria induced by HRG/TGZ potentially contributes to HRG/TGZ-induced cell death.

N-Acetylcysteine (NAC) interacts with ROS and oxygen radicals, counteracting ROS-induced effects. To test whether the augmented ROS level indeed plays a role in mediating the HRG/TGZ-induced cell death, MCF-7 cells were pretreated with NAC and then challenged with a combination of HRG and TGZ. NAC was able to significantly protect cells from HRG/TGZ-induced cell death (Fig. 5*a*), indicating that the generation of ROS is one of major determinants of HRG/TGZ-induced cell death.

Although apoptotic cell death accounted for a minor portion of HRG/TGZ-induced cell death (Fig. 3*b*), NAC attenuated nuclear DNA fragmentation (apoptosis) induced by HRG/TGZ by about 40–50% (Fig. 5*b*), suggesting that ROS actively take part in HRG/TGZ-induced apoptotic cell death. This protective effect of NAC against HRG/TGZ-induced cell death was accompanied with the inhibition of the late phase p38 MAPK activation (Fig. 5*c*). Interestingly, SB 203580 was also able to reduce the level of ROS in HRG/TGZ-treated cells (supplemental Fig. 2). These results suggest that p38 MAPK and ROS can function independently or in parallel in HRG/TGZ-induced cell death, although it remains uncertain how exactly ROS and p38 MAPK are interconnected in HRG/TGZ-induced cell death.

To further substantiate the role of ROS in HRG/TGZ-induced apoptosis, MCF-7 cells were transduced with recombinant adenovirus encoding catalase. Whereas treatment with HRG/TGZ in control adenovirus-infected cells (Ad-GFP) still allowed for significant PARP cleavage, infection with catalase-encoding adenovirus (Ad-catalase) led to a reduction in PARP cleavage (Fig. 5*d*).

Recent studies indicate that autophagy plays an active role in cell death and survival (34). Whether autophagy favors apoptosis or survival is context-dependent (35). Many cellular stresses that induce ROS generation also induce autophagy, which in turn triggers or delays cell death (36). To test whether the cell death induced by HRG/TGZ is attributable to autophagy formation upon HRG/TGZ treatment, we assessed autophagy formation by immunocytochemical analysis. The quantitative analysis of LC3 revealed a significant increase in the number of LC-3 positive puncta in HRG/TGZ-treated cells compared with untreated control cells (95 ± 3 *versus* $10 \pm 2\%$, $p < 0.01$) (Fig. 5*e*). The proportion of LC3II increases during autophagosome formation, and thus its levels can serve as an indicator of autophagosome (37). HRG/TGZ induced a significant increase in LC3II expression, whereas HRG or TGZ alone had only a marginal effect on LC3II expression (Fig. 5*f*). To assess more precisely that HRG/TGZ regulates autophagic flux, MCF-7 cells were treated with the combination of E64D and pepstatin A, and the levels of LC3-II were measured. E64D/pepstatin A further increased the levels of LC3-II (supplemental Fig. 3), suggesting that HRG/TGZ induces autophagosome formation. In agreement, electron microscopic analysis revealed a number of autophagosomes in HRG/TGZ-treated cells (Fig. 5*g*).

Despite the increase in autophagy in HRG/TGZ-treated cells, this pathway does not seem to contribute significantly to HRG/TGZ-induced cell death, because inhibition of autophagy with 3-MA (at a dose that does not compromise the viability of MCF-7 cells) caused only a modest change in HRG/TGZ-induced cell death (Fig. 3*b*). Similarly, another autophagosome inhibitor, bafilomycin A, did not have a noticeable effect on the HRG/TGZ-induced cell death (data not shown). However, like most pharmacological inhibitors, 3-MA and bafilomycin A are not specific inhibitors for autophagy. To determine more precisely the role of autophagosome in HRG/TGZ-induced cell death, MCF-7 cells were transiently transfected with negative control siRNA (scramble siRNA) or Atg7 siRNA. siRNA-mediated knockdown of Atg7 markedly reduced its

FIGURE 2. **Signaling pathways in HRG/TGZ-induced breast cancer cell death.** *a,* MCF-7 cells were treated as described in the legend to Fig. 1. Cells were harvested at indicated times post-treatment, and cell lysates were then analyzed by Western blot for phosphorylated and total cellular proteins using specific antibodies as indicated. *C,* control, untreated cells; *H,* HRG; *T,* TGZ; *HT,* HRG and TGZ. Representative data from one of three independent experiments are shown. *b,* effect of p38 MAPK inhibitor (SB 203580) on HRG/TGZ-induced apoptotic cell death. MCF-7 cells were treated with combination of HRG and TGZ in the absence (HRG/TGZ (*HT*)) or presence of 4 μM SB 203580 (*HT*+*SB*). DNA fragmentation, which represents one of the hallmarks of apoptosis, was quantitated using the cell death detection ELISA kit (Roche Applied Science). The enrichment factor was used as a parameter of apoptosis. The rate of apoptosis is reflected by the enrichment of mono- and oligonucleosomes released into the cytoplasm shown on the *y* axis; an enrichment factor of 1 is equivalent to background apoptosis. The enrichment factor was calculated as the ratio between the absorbance measurements of treated cells and the basal value (untreated control cells). Data represent the mean ± S.E. from three experiments performed in duplicate. *c,* blockade of the late phase of p38 MAPK activation provides more protection from HRG/TGZ-induced apoptosis than the early phase blockade. To block the early phase p38 MAPK activation, MCF-7 cells were pretreated with p38 MAPK inhibitor (SB 203580, 4 μM) for 1 h, and then the media were replaced with fresh media containing HRG/TGZ and 4 μM SB 203580. After 5 h, the incubation medium was removed, and the cells were washed twice to get rid of SB 203580. Cells were then cultured in media containing HRG/TGZ until 48 h after initial HRG/TGZ treatment. Note that p38 MAPK activity is reversible if SB 203580 is removed. To block the late phase p38 MAPK activation, 4 μM SB 203580 was treated after the early phase p38 MAPK activation (5 h after HRG/TGZ treatment). Note that cell lysates were analyzed at 48 h after initial HRG/TGZ treatment, and thus p38 MAPK activity shown in this figure (*P-p38 MAPK*) represents the late phase p38 MAPK activity. Data shown are representative of three independent experiments. *d,* MCF-7 cells were transiently transfected with the reporter plasmid containing the PPAR-response element and internal control (pRL-SV40). The reporter-transfected cells were then incubated with each compound as indicated. The data were normalized to the *Renilla* luciferase and expressed as fold increase relative to that of control cells. Data represent the mean ± S.E. from three experiments performed in duplicate. *C,* control, untreated cells; *H,* HRG; *T,* TGZ; *HT,* HRG and TGZ.

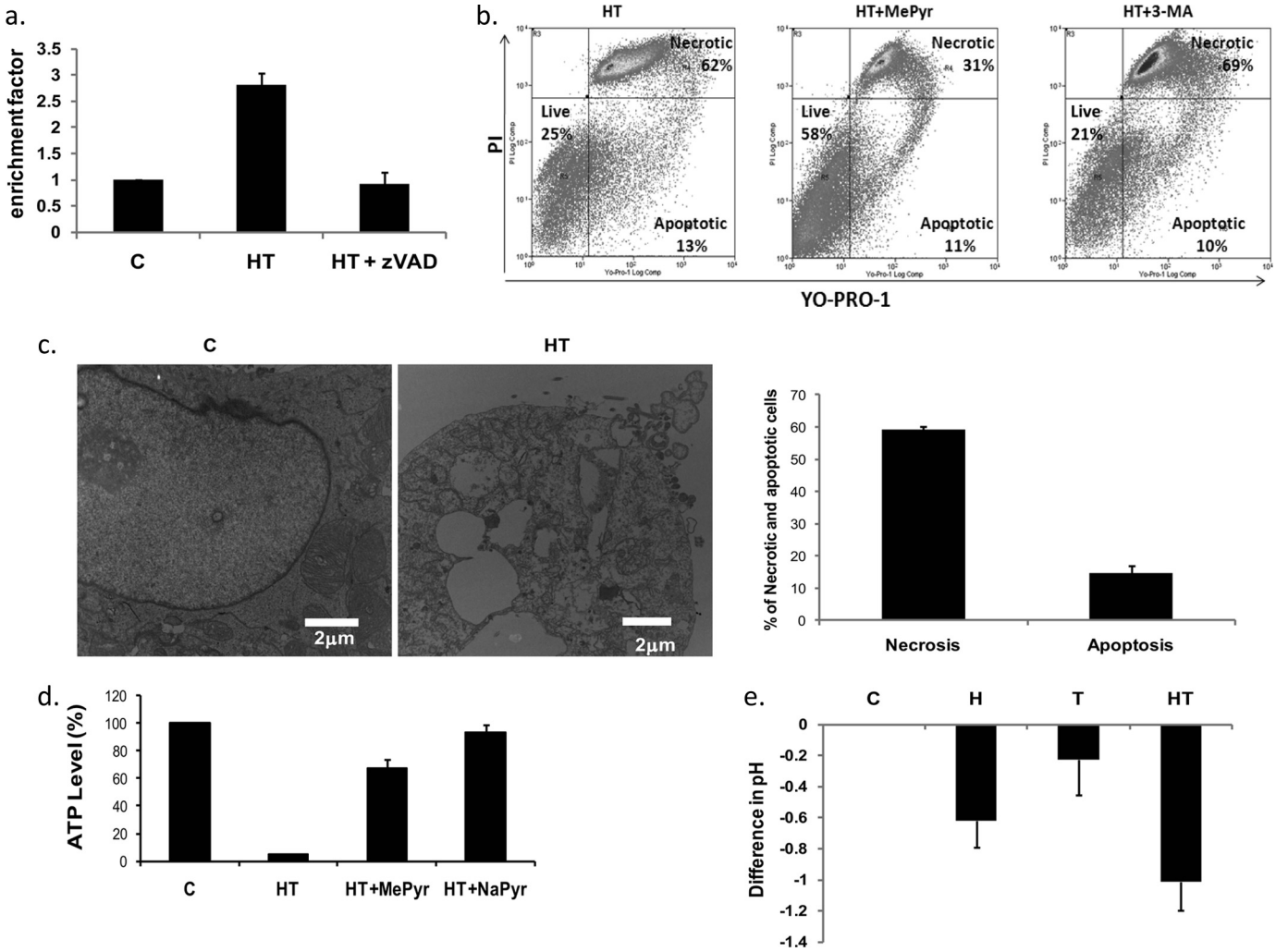

FIGURE 3. **HRG/TGZ induces both apoptotic and nonapoptotic/necrotic cell death but the primary mode is necrosis.** *a,* effect of Z-VAD-fmk on HRG/TGZ-induced apoptotic cell death. MCF-7 cells were treated with HRG and TGZ in the absence (*HT*) or presence (*HT*+*zVAD*) of 20 μM Z-VAD-fmk. Cell death detection ELISA was used to measure apoptotic cell death. Rate of apoptosis is reflected by the enrichment of nucleosomes released in each sample. The enrichment factor was calculated as described in Fig. 2*b* legend. Data represent the mean ± S.E. from three independent experiments performed in duplicate. *b,* MCF-7 cells were pretreated with 10 mM methyl pyruvate (*HT*+*MePyr*) or 10 mM 3-Methyladenine (*HT*+*3-MA*) for 1 h and then treated for 48 h with HRG and TGZ. Cells were then stained with YO-PRO-1 and PI and analyzed by flow cytometry. Plots are representative from two independent experiments. *c,* electron microscopy of HRG/TGZ-treated MCF-7 cells. MCF-7 cells were either left untreated (*C*) or treated (*HT*) for 48 h with HRG/TGZ. Cells were fixed in glutaraldehyde and examined under an electron microscope. *Bar* represents 2 μm. The accompanying graph (*right panel*) shows the electron microscopic quantitation of apoptotic and necrotic cells. The percentages of cell numbers showing apoptosis- and necrosis-like morphological changes were calculated by counting ~200 cells from randomly selected areas (>90 fields). Results are presented as mean ± S.E. ($p < 0.01$). *d,* effect of HRG/TGZ treatment on intracellular ATP level. MCF-7 cells were either left untreated (*C*) or treated for 48 h with 10 mM methyl pyruvate (*HT*+*MePyr*) or with 10 mM sodium pyruvate (*HT*+*NaPyr*) in the presence of HRG/TGZ (*HT*). ATP level was measured using a luminescence ATP detection system as described under "Experimental Procedures." Luminescence was measured as counts/s (*cps*) and normalized to total protein concentration for each sample. The relative ATP level was calculated by dividing the normalized cps of the treated samples by that of the control samples. *Bars* correspond to means ± S.E. from at least five independent experiments carried out in duplicate. *e,* MCF-7 cells were treated for 48 h with the indicated compounds and the pH of media was measured. Data are representative of at least three independent experiments. *C,* control, untreated cells; *H,* HRG; *T,* TGZ; *HT,* HRG and TGZ.

protein expression in MCF-7 cells (Fig. 5*h*, *left, top panel*). As expected, Atg7 knockdown resulted in decreased expression of LC3-II (Fig. 5*h*, *left, middle panel*). However, despite a significant "knockdown" of the Atg 7 protein, there were no noticeable differences in HRG/TGZ-induced cell death between Atg7 siRNA and control siRNA cells (Fig. 5*h*, *right panel*), indicating that autophagosome plays a minimal role in HRG/TGZ-induced cell death. Of note, treatment of NAC reduced LC3II expression, suggesting that HRG/TGZ-induced autophagy is in part due to oxidative stress (Fig. 5*f*).

Given the fact that ROS can cause damage to macromolecules such as DNA (38), we determined whether the elevated level of ROS from HRG/TGZ-treated breast cancer cells causes DNA damage. We measured γ-H2AX foci formation, a sensitive marker for double strand breaks, to visualize and quantify double strand breaks elicited by different treatment groups. HRG induced a modest increase in γ-H2AX foci formation (Fig. 6*a*). The HRG and TGZ combination, which causes an accumulation of a higher level of ROS (Fig. 4*b*), produced more γ-H2AX foci as shown in Fig. 6*a*. Western blot analysis also revealed an increase in the level of γ-H2AX in HRG/TGZ-treated cells (Fig. 6*b*, *left panel*). NAC treatment resulted in the inhibition of γ-H2AX expression (Fig. 6*b*, *right panel*), indicating that the elevated level of ROS by

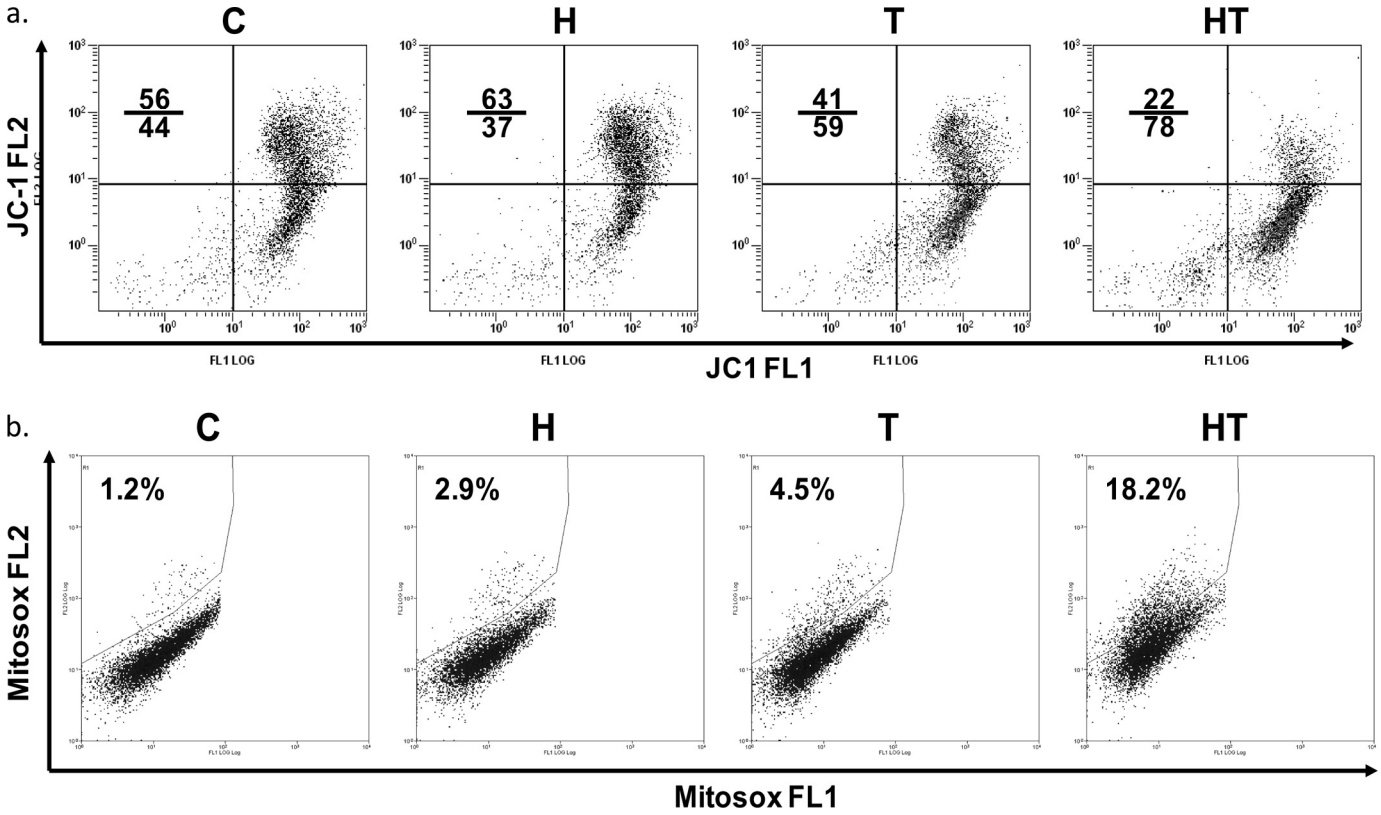

FIGURE 4. **HRG/TGZ treatment results in increased superoxide production and loss of mitochondrial membrane potential.** *a,* MCF-7 cells were cultured for 24 h with each compound as indicated. Cells were then stained with JC-1 mitochondrial membrane potential detection kit for 10 min and analyzed by flow cytometry. Cells with intact mitochondrial membrane potential are found in the *top right quadrant* of the plots. Cells with impaired mitochondrial membrane potential are found in the *low right quadrant* of the plots. Note the shift to the *lower right part* of the quadrants in HRG/TGZ (*HT*)-treated cells. *Numbers* indicate the percentage of cells in the upper and lower quadrant. Representative data from one of three independent experiments are shown. *b,* to measure mitochondrial ROS, MCF-7 cells were treated for 16 h with the indicated compounds and stained with MitoSOX Red. Gates to determine percent MitoSOX-positive cells were set to exclude 95–98% of control cells (*C,* untreated). *Numbers* in the *upper left* of each dot blot indicate the percentage of cells staining positively with MitoSOX Red. A representative blot is shown. *C,* control, untreated cells; *H,* HRG; *T,* TGZ; *HT,* HRG and TGZ.

HRG/TGZ treatment is associated with the increased γ-H2AX foci.

DISCUSSION

It has been found that HRG confers resistance against drugs such as gefitinib and tamoxifen (5), indicating that increased expression of HRG correlates with poor prognosis in breast cancer (2, 6, 39). On the contrary, this study suggests that HRG expression in breast cancer can actually be beneficial when it comes to treating breast cancer with PPARγ ligands.

We demonstrated here that HRG in combination with TGZ consistently induced massive cell death in breast cancer cells. Although the combination was equally potent in inducing cell death in all three breast cancer cell lines tested, MCF-10A cells were significantly more resistant to HRG/TGZ-induced cell death. The mechanisms underlying the resistance of MCF-10A cells against HRG/TGZ treatment are not known yet. Little or no expression of HER-4 in MCF-10A cells may account for the resistance to HRG/TGZ. However, MDA-MB-453 and SKBR-3 cells, which also express low level or absent HER-4 (40), still underwent significant cell death in response to HRG/TGZ treatment, excluding this possibility. Whether normal primary breast epithelial cells also exhibit resistance to HRG/TGZ clearly warrants further investigation.

p38 MAPK inhibitor, but not PI3-K/AKT, JNK, or MEK/ERK inhibitors, reduced the capacity of HRG/TGZ to trigger apoptosis, suggesting that p38 MAPK plays a role in HRG/TGZ-induced apoptosis. HRG/TGZ treatment elicited a biphasic pattern of p38 MAPK activation (early phase and late phase). Importantly, the late phase activation seems to play a more significant role than the early phase activation in HRG/TGZ-mediated apoptosis, because the selective blocking of the late phase p38 MAPK activation provided a substantially higher level of protection against HRG/TGZ-induced apoptosis than that obtained by the early phase blocking. However, in either case, p38 MAPK inhibitor cannot fully protect breast cancer cells from HRG/TGZ-induced apoptosis, suggesting that alternative pathways to trigger cell death may exist.

Activation of the PPARγ pathway is known to induce apoptosis, but although HRG/TGZ synergistically increased in the transcriptional activity of the PPRE luciferase reporter, GW9662 (PPARγ antagonist) treatment showed no effect on HRG/TGZ-induced cell death, indicating that the observed effects are independent of PPARγ activation. It is known that thiazolidinediones can induce their cytotoxic activity independent of PPARγ activation. However, the molecular basis of how thiazolidinediones exert their effects in a PPARγ-independent manner is currently incompletely elucidated (41).

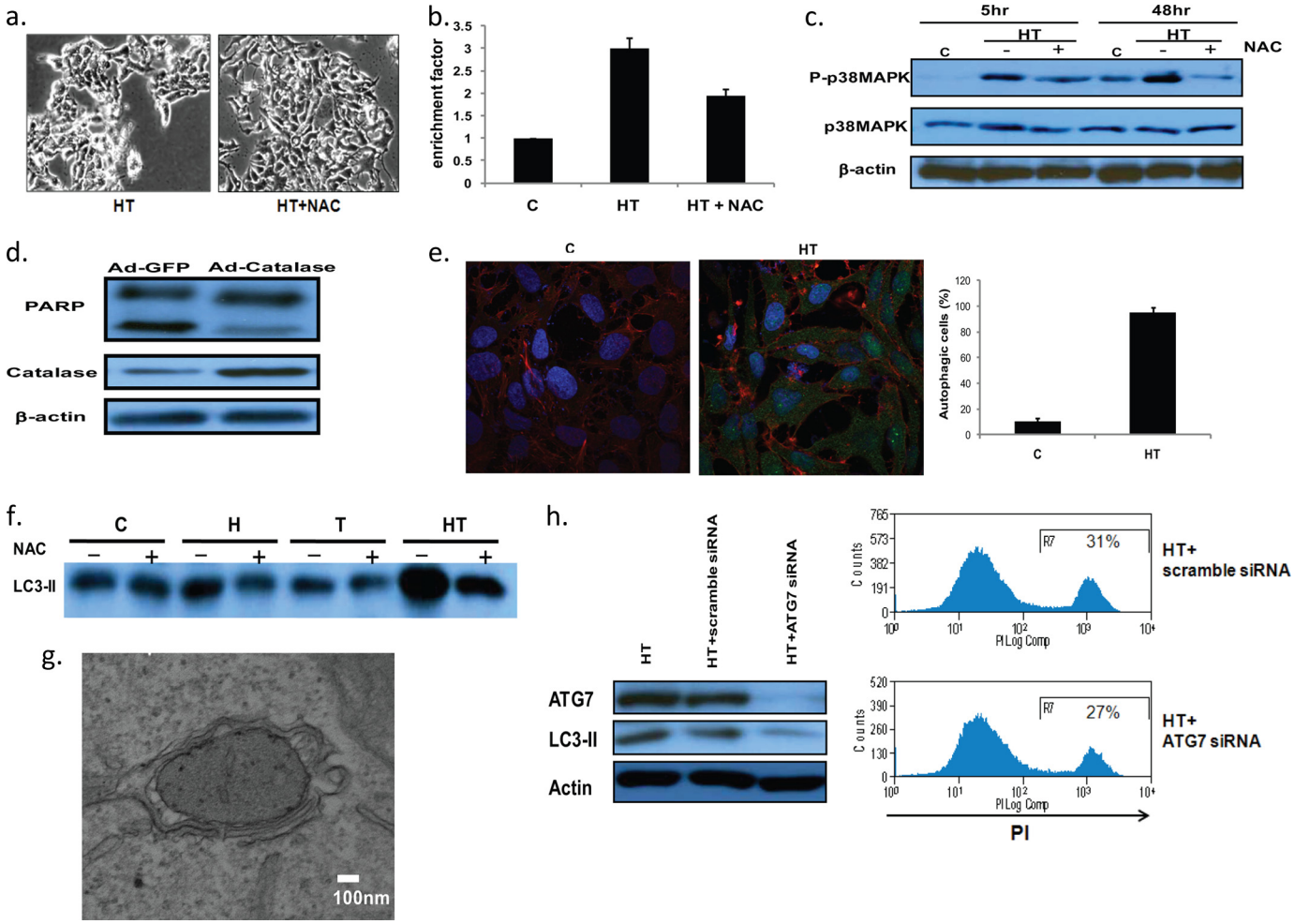

FIGURE 5. **Antioxidants NAC and catalase protect cells from the cell death induced by HRG/TGZ.** *a,* effect of NAC on HRG/TGZ-induced cell death. Phase contrast images of cells treated with HRG/TGZ (*HT*) and HRG/TGZ+NAC (*HT+NAC*) are shown. *b,* effect of NAC on HRG/TGZ-induced apoptosis. NAC (5 mM) was pretreated for 1 h before HRG/TGZ treatment. After 48 h of HRG/TGZ treatment, cell death detection ELISA was used to measure apoptotic cell death. The enrichment factor was calculated as described in Fig. 2 legend. Data represent the mean ± S.E. from three experiments performed in duplicate. *c,* cells were treated with HRG/TGZ in the presence (+) or absence (−) of NAC under similar cell culture conditions as described above. Cells were collected at 48 h after HRG/TGZ treatment and analyzed for p38 MAPK phosphorylation by Western blot. *d,* effect of catalase on HRG/TGZ-induced PARP cleavage. MCF-7 cells were transduced with adenoviral vectors encoding catalase (*Ad-catalase*) or empty vector (*Ad-GFP*) as a control. Transduction of cells by Ad-GFP or Ad-catalase was confirmed by GFP expression (at least 80% of transduction efficiency is based on GFP expression). Transduced cells were then treated with HRG/TGZ for 36 h, and the level of PARP cleavage was measured. *e,* MCF-7 cells grown on glass coverslips were treated as indicated. Cells were stained with antibodies to LC3 (*green*), cytokeratin (*red*), and DAPI (*blue*). The number of cells with a punctate LC3 pattern was quantified by counting more than 100 cells from at least three randomly selected fields, and the results represent the mean ± S.E. ($p < 0.01$). *f,* MCF-7 cells were cultured with each compound as indicated in the presence (+) or absence (−) of NAC. Cells were then analyzed for the levels of LC3II. *C,* control, untreated cells; *H,* HRG; *T, TGZ*; *HT,* HRG and TGZ. *g,* formation of autophagosomes was confirmed through electron microscopy. MCF-7 cells were treated for 48 h with HRG/TGZ. Cells were then fixed and examined as described in Fig. 3*c*. At a high magnification, HRG/TGZ-treated cells exhibited typical morphological features of autophagy. *Bar* represents 100 nm. *h, left panel,* MCF-7 cells transfected with either scrambled control siRNA (*HT+scramble siRNA*) or ATG7 siRNA (*HT+ATG7 siRNA*) were treated with HRG/TGZ for 48 h. Cell lysates were then analyzed by immunoblot analysis with the anti-ATG7 or LC3II antibody. *Right panel,* MCF-7 cells were transfected with siRNAs as indicated and treated with HRG/TGZ for 30–36 h. Cell death was analyzed by PI staining as described in the legend to Fig. 1. *Numbers* indicate the percentage of PI-positive cells. Please note that cells were retrieved for PI staining at an earlier time point (30–36 h after HRG/TGZ treatment) and thus showed lower level of cell death compared with corresponding cells treated for 48 h.

Importantly, inhibition of caspase activity with a pan-caspase inhibitor provided only modest protection against HRG/TGZ-induced cell death. Although necrosis accounted for the majority of HRG/TGZ-induced cell death, necrotic and apoptotic cell death was concomitantly activated in HRG/TGZ-treated cells. It was consistently observed that HRG/TGZ-treated media turned yellow during cell death, suggesting HRG/TGZ-induced cell death could be the consequence of a metabolic stress. Consistent with this speculation, pyruvate addition significantly protected cells from HRG/TGZ-induced cell death. Transport of nutrients from extracellular medium into the cell is mediated by specific transporter proteins. For example, IL-3 withdrawal or ceramide treatment induces cell death by down-regulating nutrient transporters (42, 43). Accordingly, only a permeable pyruvate (MePyr), but not an impermeable pyruvate (NaPyr), could counteract the onset of metabolic stress in ceramide-treated cells (43). In contrast, sodium pyruvate could exert a protective effect against the HRG/TGZ-induced cell death (data not shown). This result suggests that HRG/TGZ-induced cell death is not due to down-regulation of nutrient transporter proteins. These protective effects of pyruvate

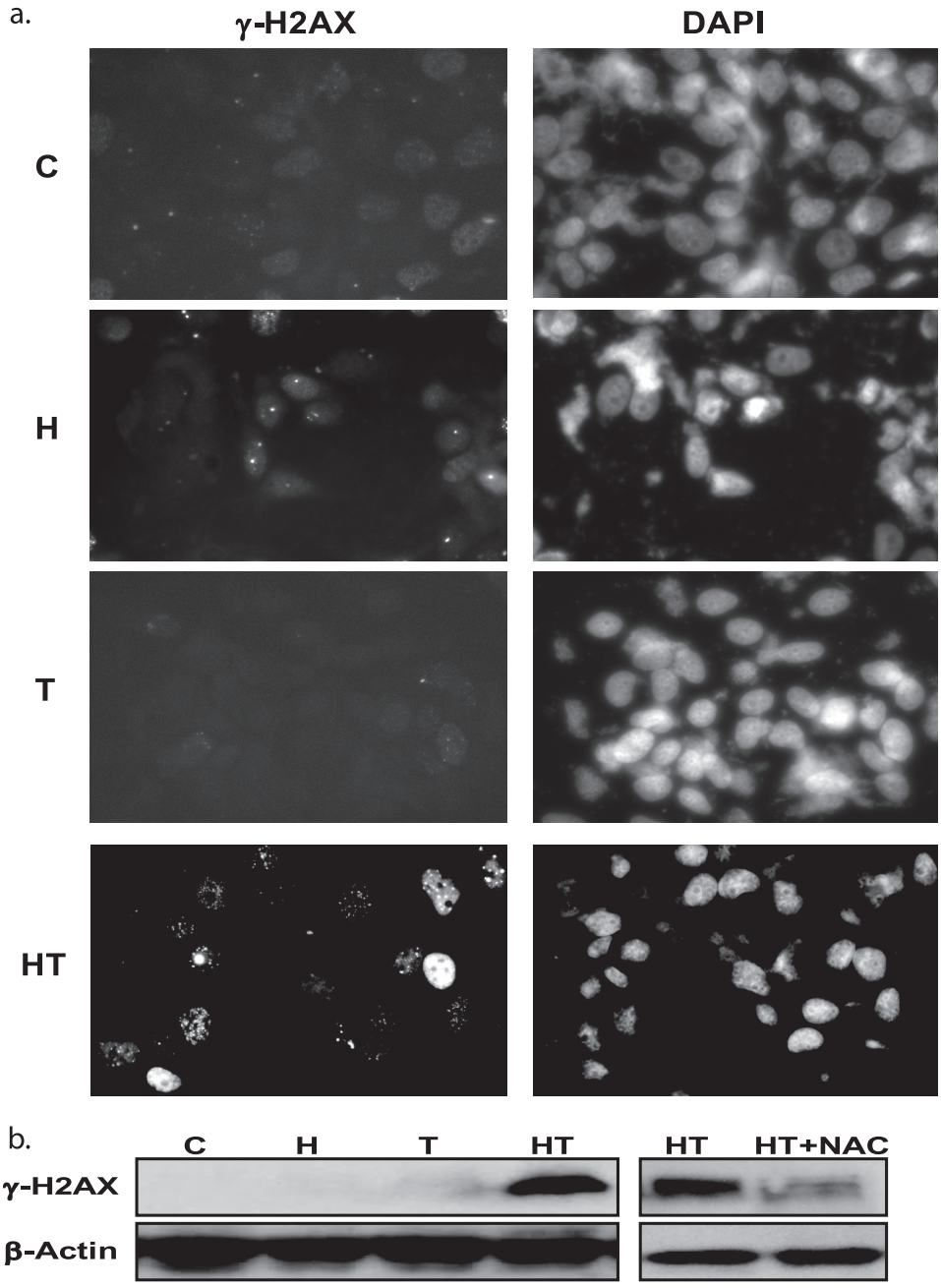

FIGURE 6. **HRG/TGZ induces DNA damage through oxidative stress.** *a,* immunocytochemical staining of γ-H2AX was performed as described under "Experimental Procedures." MCF-7 cells were incubated with the indicated compounds for 40 h. They were then stained for the presence of phosphorylated γ-H2AX (*left panels*). The nuclei were visualized by DAPI staining (*right panels*). A representative image is shown. *C,* control, untreated cells; *H,* HRG; *T,* TGZI; *HT,* HRG and TGZ. *b,* MCF-7 cells were incubated for 40 h with the indicated compounds. Cell lysates were analyzed by Western blot for the expression of phosphorylated γ-H2AX. *C,* control, untreated cells; *H,* HRG; *T,* TGZ; *HT,* HRG and TGZ.

(NaPyr and MePyr) could be multifactorial, including scavenging ROS and/or providing an energy source, etc. (44–46). Although further studies are necessary to explore such possibilities, our study showed that pyruvate significantly attenuated the decline in ATP levels in HRG/TGZ-treated cells, suggesting that pyruvate was used as an energy substrate during HRG/TGZ-induced metabolic stress.

Direct measurement of mitochondrial ROS showed an accumulation of higher levels of superoxide in HRG/TGZ-treated cells, and this was apparently correlated with impaired mitochondrial function. Thus, it is likely that oxidative damage to mitochondria is associated with HRG/TGZ-induced cell death. ROS are also well known to cause DNA damage and induce cytotoxicity. HRG/TGZ treatment triggered a pronounced increase in γ-H2AX levels compared with either treatment alone, but pretreatment with NAC reduced γ-H2AX levels, indicating that HRG/TGZ-induced DNA damage represents a ROS-dependent process.

Although HRG/TGZ treatment increased autophagosome formation, suppression of autophagosomes did not significantly affect HRG/TGZ-induced cell death. These results suggest that autophagosome formation, although it is markedly

increased upon HRG/TGZ treatment, is not sufficient to override HRG/TGZ-induced cell death.

Whereas HRG signaling exerts stimulatory effects on breast cancer cells (2, 6, 39), there are also contradictory results showing that activation of HRG signaling exerts inhibitory effects on breast cancer cell growth and survival (1, 29, 47). When, how, and in which conditions HRG functions as stimulatory or inhibitory molecules in breast cancer cells is not clearly understood (48). Some studies suggest that HRG can either promote proliferation or induce apoptosis depending on HRG concentration (49). However, when cell death was assessed with various amounts of HRG in the presence of 10 μM TGZ, there was no apparent correlation between HRG concentrations and the extent of HRG/TGZ-induced cell death.[3]

When MCF-7 cells were treated with a fixed dose of HRG (100 ng/ml) with varying concentrations of TGZ, the level of HRG/TGZ-induced cell death was noticeably reduced at concentrations lower than 10 μM TGZ (supplemental Fig. 4). Previous studies showed that a higher concentration of TGZ (40 μM) is needed to achieve 30–50% of cell death in MCF-7 cells (50, 51). Meanwhile, our study found that a significantly lower concentration of TGZ (10 μM), when it is combined with HRG, was sufficient to induce 85–95% (if not all) of cell death (at 72 h post-treatment) in MCF-7 cells. Although further detailed pharmacokinetic studies are required to determine optimal doses of each of the agents, lowering the dose of PPARγ agonists would be beneficial to maximize their therapeutic potential and minimize the side effects.

The level of ErbB2 expression is also known to be correlated with HRG-induced cell death (52). However, HRG/TGZ combination induced a similar degree of cell death both in ErbB2 high (SKBR-3 and MDA-MB-453) and low expressing cells (MCF-7), suggesting that the level of ErbB2 does not play a crucial role in HRG/TGZ-induced cell death. Therefore, neither the level of *ErbB2* expression nor HRG concentration seems to be the major determinant in mediating HRG/TGZ-induced cell death.

Evasion from apoptosis is common in cancer cells and remains a major obstacle to the effective treatment of breast cancer. However, apoptosis-resistant cancer cells may still remain sensitive to necrotic cell death, and diverting the mode of cell death from the apoptotic toward the necrotic is one of the promising therapeutic approaches for therapy-resistant tumors (53). Nevertheless, necrotic cell death results in the release of cellular contents, and this is often associated with inflammation and tumor growth (54, 55). Therefore, the therapeutic enhancement of necrotic cell death should be carefully weighed along with the potential adverse effects.

Our data suggest that metabolic stress is implicated in HRG/TGZ-induced cell death. In this scenario, HRG/TGZ treatment evokes metabolic stress that would promote cellular oxidative stress by increasing ROS formation. Excessive ROS leads to mitochondrial dysfunction and impairs energy metabolism, and this, in turn, further aggravates a bioenergetic crisis. As a drastic decrease in cellular energy status can switch the cell death mode from apoptosis to necrosis (56), it is possible that exaggerated energy demand by HRG/TGZ-treated cells can drive cells into necrotic cell death. Alternatively, it is possible that HRG makes breast cancer cells more susceptible to TGZ or vice versa.

With the heterogeneity of breast cancer, identification of specific combinatorial treatment is an important task to tailor the therapy best suited to the individual patient. In this regard, the combination of HRG with TGZ may provide the basis for a novel strategy in the treatment of apoptosis-resistant and/or hormone-refractory breast cancer.

Acknowledgments—We thank Drs. Hannah Rabinowich, Merrill Egorin, and Shivendra Singh for advice and discussion and Dr. Sally Morton for critical reading of this manuscript. We also thank the reviewers for constructive suggestions.

[3] B.-H. Park and B.-C. Lee, unpublished results.

REFERENCES

1. Le, X. F., Varela, C. R., and Bast, R. C., Jr. (2002) *Apoptosis* **7,** 483–491
2. Lupu, R., Cardillo, M., Cho, C., Harris, L., Hijazi, M., Perez, C., Rosenberg, K., Yang, D., and Tang, C. (1996) *Breast Cancer Res. Treat.* **38,** 57–66
3. Vadlamudi, R., Adam, L., Tseng, B., Costa, L., and Kumar, R. (1999) *Cancer Res.* **59,** 2843–2846
4. Xu, F., Yu, Y., Le, X. F., Boyer, C., Mills, G. B., and Bast, R. C., Jr. (1999) *Clin. Cancer Res.* **5,** 3653–3660
5. Hutcheson, I. R., Knowlden, J. M., Hiscox, S. E., Barrow, D., Gee, J. M., Robertson, J. F., Ellis, I. O., and Nicholson, R. I. (2007) *Breast Cancer Res.* **9,** R50
6. Atlas, E., Cardillo, M., Mehmi, I., Zahedkargaran, H., Tang, C., and Lupu, R. (2003) *Mol. Cancer Res.* **1,** 165–175
7. Michalik, L., Desvergne, B., and Wahli, W. (2004) *Nat. Rev. Cancer* **4,** 61–70
8. Yoshizawa, K., Cioca, D. P., Kawa, S., Tanaka, E., and Kiyosawa, K. (2002) *Cancer* **95,** 2243–2251
9. Mueller, E., Sarraf, P., Tontonoz, P., Evans, R. M., Martin, K. J., Zhang, M., Fletcher, C., Singer, S., and Spiegelman, B. M. (1998) *Mol. Cell* **1,** 465–470
10. Nicol, C. J., Yoon, M., Ward, J. M., Yamashita, M., Fukamachi, K., Peters, J. M., and Gonzalez, F. J. (2004) *Carcinogenesis* **25,** 1747–1755
11. Mehta, R. G., Williamson, E., Patel, M. K., and Koeffler, H. P. (2000) *J. Natl. Cancer Inst.* **92,** 418–423
12. Sarraf, P., Mueller, E., Jones, D., King, F. J., DeAngelo, D. J., Partridge, J. B., Holden, S. A., Chen, L. B., Singer, S., Fletcher, C., and Spiegelman, B. M. (1998) *Nat. Med.* **4,** 1046–1052
13. Saez, E., Tontonoz, P., Nelson, M. C., Alvarez, J. G., Ming, U. T., Baird, S. M., Thomazy, V. A., and Evans, R. M. (1998) *Nat. Med.* **4,** 1058–1061
14. Lefebvre, A. M., Chen, I., Desreumaux, P., Najib, J., Fruchart, J. C., Geboes, K., Briggs, M., Heyman, R., and Auwerx, J. (1998) *Nat. Med.* **4,** 1053–1057
15. Saez, E., Rosenfeld, J., Livolsi, A., Olson, P., Lombardo, E., Nelson, M., Banayo, E., Cardiff, R. D., Izpisua-Belmonte, J. C., and Evans, R. M. (2004) *Genes Dev.* **18,** 528–540
16. Lucarelli, E., Sangiorgi, L., Maini, V., Lattanzi, G., Marmiroli, S., Reggiani, M., Mordenti, M., Alessandra Gobbi, G., Scrimieri, F., Zambon Bertoja, A., and Picci, P. (2002) *Int. J. Cancer* **98,** 344–351
17. Burstein, H. J., Demetri, G. D., Mueller, E., Sarraf, P., Spiegelman, B. M., and Winer, E. P. (2003) *Breast Cancer Res. Treat.* **79,** 391–397
18. Kulke, M. H., Demetri, G. D., Sharpless, N. E., Ryan, D. P., Shivdasani, R., Clark, J. S., Spiegelman, B. M., Kim, H., Mayer, R. J., and Fuchs, C. S. (2002) *Cancer J.* **8,** 395–399
19. Girnun, G. D., Naseri, E., Vafai, S. B., Qu, L., Szwaya, J. D., Bronson, R., Alberta, J. A., and Spiegelman, B. M. (2007) *Cancer Cell* **11,** 395–406
20. Kelland, L. (2007) *Nat. Rev. Cancer* **7,** 573–584
21. Sirohi, B., Arnedos, M., Popat, S., Ashley, S., Nerurkar, A., Walsh, G., Johnston, S., and Smith, I. E. (2008) *Ann. Oncol.* **19,** 1847–1852
22. Kulms, D., Pöppelmann, B., Yarosh, D., Luger, T. A., Krutmann, J., and

Schwarz, T. (1999) *Proc. Natl. Acad. Sci. U.S.A.* **96,** 7974–7979
23. Lunardi, C., Dolcino, M., Peterlana, D., Bason, C., Navone, R., Tamassia, N., Tinazzi, E., Beri, R., Corrocher, R., and Puccetti, A. (2007) *PLoS One* **2,** e473
24. Blanchard, F., Rusiniak, M. E., Sharma, K., Sun, X., Todorov, I., Castellano, M. M., Gutierrez, C., Baumann, H., and Burhans, W. C. (2002) *Mol. Biol. Cell* **13,** 1536–1549
25. Gawlitta, D., Oomens, C. W., Baaijens, F. P., and Bouten, C. V. (2004) *Cytotechnology* **46,** 139–150
26. Han, J., Hou, W., Goldstein, L. A., Lu, C., Stolz, D. B., Yin, X. M., and Rabinowich, H. (2008) *J. Biol. Chem.* **283,** 19665–19677
27. Uehara, N., Matsuoka, Y., and Tsubura, A. (2008) *Mol. Cancer Res.* **6,** 186–193
28. Sun, H., Berquin, I. M., and Edwards, I. J. (2005) *Cancer Res.* **65,** 4442–4447
29. Daly, J. M., Olayioye, M. A., Wong, A. M., Neve, R., Lane, H. A., Maurer, F. G., and Hynes, N. E. (1999) *Oncogene* **18,** 3440–3451
30. Mackay, K., and Mochly-Rosen, D. (1999) *J. Biol. Chem.* **274,** 6272–6279
31. Martin, G., Sabido, O., Durand, P., and Levy, R. (2004) *Biol. Reprod.* **71,** 28–37
32. Lin, M. T., and Beal, M. F. (2006) *Nature* **443,** 787–795
33. Power, C. P., Wang, J. H., Manning, B., Kell, M. R., Aherne, N. J., Aherne, N. F., Wu, Q. D., and Redmond, H. P. (2004) *J. Immunol.* **173,** 5229–5237
34. Liu, Z., and Lenardo, M. J. (2007) *Dev. Cell* **12,** 484–485
35. Fung, C., Lock, R., Gao, S., Salas, E., and Debnath, J. (2008) *Mol. Biol. Cell* **19,** 797–806
36. Scherz-Shouval, R., and Elazar, Z. (2007) *Trends Cell Biol.* **17,** 422–427
37. Kabeya, Y., Mizushima, N., Ueno, T., Yamamoto, A., Kirisako, T., Noda, T., Kominami, E., Ohsumi, Y., and Yoshimori, T. (2000) *EMBO J.* **19,** 5720–5728
38. Cooke, M. S., Evans, M. D., Dizdaroglu, M., and Lunec, J. (2003) *FASEB J.* **17,** 1195–1214
39. Krane, I. M., and Leder, P. (1996) *Oncogene* **12,** 1781–1788
40. Boone, J. J., Bhosle, J., Tilby, M. J., Hartley, J. A., and Hochhauser, D. (2009) *Mol. Cancer Ther.* **8,** 3015–3023
41. Blanquicett, C., Roman, J., and Hart, C. M. (2008) *Cancer Ther.* **6,** 25–34
42. Lum, J. J., Bauer, D. E., Kong, M., Harris, M. H., Li, C., Lindsten, T., and Thompson, C. B. (2005) *Cell* **120,** 237–248
43. Guenther, G. G., Peralta, E. R., Rosales, K. R., Wong, S. Y., Siskind, L. J., and Edinger, A. L. (2008) *Proc. Natl. Acad. Sci. U.S.A.* **105,** 17402–17407
44. Izumi, Y., Benz, A. M., Katsuki, H., and Zorumski, C. F. (1997) *J. Neurosci.* **17,** 9448–9457
45. Giandomenico, A. R., Cerniglia, G. E., Biaglow, J. E., Stevens, C. W., and Koch, C. J. (1997) *Free Radic. Biol. Med.* **23,** 426–434
46. Salahudeen, A. K., Clark, E. C., and Nath, K. A. (1991) *J. Clin. Invest.* **88,** 1886–1893
47. Le, X. F., Marcelli, M., McWatters, A., Nan, B., Mills, G. B., O'Brian, C. A., and Bast, R. C., Jr. (2001) *Oncogene* **20,** 8258–8269
48. Breuleux, M. (2007) *Cell. Mol. Life Sci.* **64,** 2358–2377
49. Cardillo, M., Yankelevich, B., Mazumder, A., and Lupu, R. (1996) *Cancer Immunol. Immunother.* **43,** 19–25
50. Yin, F., Bruemmer, D., Blaschke, F., Hsueh, W. A., Law, R. E., and Herle, A. J. (2004) *Oncogene* **23,** 4614–4623
51. Yin, F., Wakino, S., Liu, Z., Kim, S., Hsueh, W. A., Collins, A. R., Van Herle, A. J., and Law, R. E. (2001) *Biochem. Biophys. Res. Commun.* **286,** 916–922
52. Le, X. F., McWatters, A., Wiener, J., Wu, J. Y., Mills, G. B., and Bast, R. C., Jr. (2000) *Clin. Cancer Res.* **6,** 260–270
53. Jin, S., DiPaola, R. S., Mathew, R., and White, E. (2007) *J. Cell Sci.* **120,** 379–383
54. Vakkila, J., and Lotze, M. T. (2004) *Nat. Rev. Immunol.* **4,** 641–648
55. Amaravadi, R. K., and Thompson, C. B. (2007) *Clin. Cancer Res.* **13,** 7271–7279
56. Leist, M., Single, B., Naumann, H., Fava, E., Simon, B., Kühnle, S., and Nicotera, P. (1999) *Exp. Cell Res.* **249,** 396–403